Journal of Nuclear Medicine, published on September 22, 2016 as doi:10.2967/jnumed.115.170910

Pharmacokinetic evaluation of the tau PET radiotracer ^{18}F-T807 (^{18}F-AV-1451) in human subjects

Dustin W. Wooten[1,2], Nicolas J. Guehl[1,2], Eline E. Verwer[1,2], Timothy M. Shoup[1,2], Daniel L. Yokell[1,2], Nevena Zubcevik[3], Neil Vasdev[1,2], Ross D. Zafonte[3,4], Keith A. Johnson[2], Georges El Fakhri[1,2], Marc D. Normandin[1,2,*]

[1]Gordon Center for Medical Imaging, [2]Division of Nuclear Medicine and Molecular Imaging, Department of Radiology, Massachusetts General Hospital, Harvard Medical School, Boston, MA

[3]Department of Physical Medicine and Rehabilitation, Spaulding Rehabilitation Hospital, Massachusetts General Hospital, [4]Brigham and Women's Hospital, Harvard Medical School, Boston, MA

First author:

Dustin W. Wooten

Massachusetts General Hospital

55 Fruit Street, White 427

Boston, MA 02114

Fax: (617) 726-6165

Phone: (617) 643-5097

dwooten@mgh.harvard.edu

* Corresponding author:

Marc D. Normandin

Massachusetts General Hospital

55 Fruit Street, White 427

Boston, MA 02114

Fax: (617) 726-6165

Phone: (617) 643-6836

normandin@mgh.harvard.edu

Keywords: Tau, PET, ^{18}F-T807, pharmacokinetics, kinetic modeling

RUNNING TITLE: ^{18}F-T807 PHARMACOKINETICS IN HUMANS

ABSTRACT

^{18}F-T807 is a PET radiotracer developed for imaging tau protein aggregates, which are implicated in neurological disorders including Alzheimer's disease (AD) and traumatic brain injury (TBI). The current study characterizes ^{18}F-T807 pharmacokinetics in human subjects using dynamic PET imaging and metabolite-corrected arterial input functions. **Methods:** Nine subjects (4 control, 3 with history of TBI, 2 mild cognitive impairment (MCI) due to suspected AD) underwent dynamic PET imaging for up to 120 minutes after bolus injection of ^{18}F-T807 with arterial blood sampling. Total volume of distribution (V_T) was estimated using compartmental modeling (one- and two-tissue configurations) and graphical analysis techniques (Logan and MA1 regression methods). Reference region-based methods of quantification were explored including Logan distribution volume ratio (DVR) and static standardized uptake value ratio (SUVR) utilizing the cerebellum as a reference tissue. **Results:** Percent unmetabolized ^{18}F-T807 in plasma followed a single exponential with $T_{1/2}$ of 17.0±4.2 minutes. Metabolite corrected plasma radioactivity concentration fit a bi-exponential ($T_{1/2}$: 18.1±5.8; 2.4±0.5 minutes). ^{18}F-T807 in gray matter peaked quickly (SUV >2 at ~5 minutes). Compartmental modeling resulted in good fits and the two-tissue model with estimated blood volume correction (2Tv) performed best, particularly in regions with elevated binding. V_T was greater in MCI subjects than controls in the occipital, parietal, and temporal cortices as well as the posterior cingulate gyrus, precuneus, and mesial temporal cortex. High focal uptake was found in the posterior corpus callosum of a TBI subject. Plots from Logan and MA1 graphical methods became linear by 30 minutes, yielding regional estimates of V_T in excellent agreement with compartmental analysis and providing high quality parametric maps when applied in voxelwise fashion. Reference region based approaches including Logan DVR (t^*=55 min) and SUVR (80-100 min interval) were highly correlated with *DVR* estimated using 2Tv (R^2=0.97, $p<0.0001$). **Conclusions:** ^{18}F-T807 showed rapid clearance from plasma and properties suitable for tau quantification with PET. Furthermore, simplified approaches utilizing DVR (t^*=55 minutes) and static SUVR (80-100 minutes) with cerebellar reference tissue were found to correlate highly with compartmental modeling outcomes.

INTRODUCTION

The tubulin-associated unit (or tau) is a naturally occurring protein that is integral in providing the white matter microtubule support structure. When impaired, tau proteins can abnormally hyperphosphorylate to form paired helical filaments and eventually insoluble aggregates (*1,2*). These neuronal changes are believed to cause decline in neuronal communication and eventual cell death. Tau pathology is a key hallmark in Alzheimer's disease (*3*) and traumatic brain injury (*4,5*). Recently, much effort has been placed in the development of PET radiotracers for in vivo quantitation of tau (*6*). Optimal radiotracer characteristics for quantification of tauopathies include selectivity for tau, low nonspecific uptake, high brain penetration, fast clearance from plasma, minimal brain penetrating radioactive metabolites, and minimal defluorination for ^{18}F-labeled compounds. Several PET radiotracers are currently in use. ^{18}F-FDDNP showed promise initially, but binding was found to be non-specific (*7*). In vivo imaging with [^{11}C]PBB3 (*8*) resulted in a radioactive metabolite was found to enter the brain complicating quantification of tau pathology (*9*). A series of compounds developed by Okamura and colleagues are showing potential. Earlier versions, THK5105 and THK5117, had relatively high levels of white matter uptake, however, the most recent compound, THK5351, is reported to exhibit less white matter retention and promising kinetics (*10,11*). Two other compounds were developed by Siemens namely ^{18}F-T807 (*12,13*) (also known as ^{18}F-AV1451) and ^{18}F-T808 (*14*). ^{18}F-T808 demonstrated high bone uptake suggestive of defluorination (*15*). ^{18}F-T807 showed favorable PET imaging properties and imaging studies showed ^{18}F-T807 uptake tracked well with expected tau pathology distribution throughout the stages of Alzheimer's disease (*12*). Due to the difficult synthesis of ^{18}F-T807 using methods initially described, our group developed a concise radiosynthesis appropriate for production on commercially available automated synthesis modules expanding the access of ^{18}F-T807 (*16*).

Binding of ^{18}F-T807 in postmortem brain tissue from a range of neurological conditions has been assessed (*17*) and research utilizing ^{18}F-T807 for in vivo imaging has been active (*18*), however a full characterization of the in vivo pharmacokinetic profile and determination of appropriate quantification methods has yet to be performed. Therefore, the goal of this work was to evaluate the pharmacokinetics of ^{18}F-T807 using dynamic PET imaging data and arterial input functions corrected for radiometabolites. In subjects demonstrating a wide range of expected tau pathology including healthy controls, subjects with MCI, and subjects with a history of traumatic brain injury, we performed compartmental modeling using arterial input functions. With the compartmental modeling estimates of

total volume of distribution (V_T) as a gold standard, we then compared simplified approaches for estimation of V_T and reference region based methods for quantitation of ^{18}F-T807 uptake.

METHODS

Subjects

As shown in table 1, nine subjects were included in this work consisting of 4 healthy controls absent neurological conditions, 2 with mild cognitive impairment (MCI), and 3 with a history of TBI (2 due to automotive accidents and 1 former professional football player with history of concussion). The study has been approved by the institutional review board at Massachusetts General Hospital, and all subjects signed an informed consent form.

--Insert Table 1 here—

Imaging Procedures

Magnetic Resonance Imaging

MRI procedures were performed for acquisition of a structural T1 weighted magnetization-prepared rapid gradient-echo (MPRAGE) (*19*) using a 3T Tim Trio (Siemens Medical Systems, Erlangen, Germany). The 3D acquisition used the following parameters: repetition time/echo time/inversion time, 2100/2.89/1100 ms, 12° flip angle, 1 mm slice thickness, matrix size 256 x 224.

Positron Emission Tomography

^{18}F-T807 was synthesized as previously described (*16*). Imaging was performed using an ECAT EXACT HR+ (CTI/Siemens, Knoxville, Tennessee, United States) in 3D acquisition mode. Emission data collection was initiated with the bolus injection of 121-196 MBq of ^{18}F-T807. Time bins were 6x10, 8x15, 6x30, 8x60, 8x120, and 6x300 seconds for the first 60 min, at which time the subjects were allowed a brief break and then repositioned on the scanner for collection of emission data from 75 up to 120 min as 9x300 sec frames. Six minute transmission scans were acquired just prior to administration of ^{18}F-T807 and immediately following the end of emission data acquisition for attenuation correction of PET images in the first and second scan blocks, respectively. ^{18}F-T807 was

administered via the antecubital vein over a one-minute infusion using a Medfusion syringe pump while arterial samples were drawn from the radial artery of the opposite arm. Arterial samples of 1-3 mL were acquired every 15 seconds immediately following radiotracer injection and decreased in frequency to every 15 minutes toward the end of the scanning duration. ^{18}F-T807 metabolism was measured from 3 mL blood samples acquired at 5, 10, 15, 30, 60, and 90 minutes.

Data Processing And Analysis

Image Processing

Dynamic PET sinograms were reconstructed using filtered backprojection while applying corrections for scatter, attenuation, deadtime, random coincident events, and scanner normalization. Final reconstructed images had voxel dimensions of 128 x 128 x 63 and voxel sizes of 2.06 x 2.06 x 2.42 mm. Motion correction was effected through frame-by-frame rigid body registration using a least squares algorithm with Levenberg-Marquardt optimization as described in (*20*).

Dynamic PET images from session two were summed and rigidly coregistered to summed images from the pre-break imaging session (part one). To derive the transformation matrix, the dynamic PET images (summed from 1 to 10 minutes after ^{18}F-T807 injection) were rigidly coregistered to the structural MPRAGE image and the MPRAGE itself was transformed into standard MNI space (*21*) using affine registration followed by nonlinear warping (FLIRT and FNIRT in FSL (*22*)). The combined transformation matrix was then applied inversely on MNI and Harvard-Oxford atlases (FSL) in order to warp the atlas based regions of interest (ROIs) into native PET space for extraction of radioactivity time activity curves (TACs). ROIs surveyed in this work are described in Supplemental Table 1 and shown in Supplemental Figure 1. To facilitate direct visual comparison between subjects, the PET images shown in the figures *were* transformed into MNI space using the derived combined transformation matrix.

Arterial Input Function

Whole blood (WB) and plasma time activity curves were obtained by linear interpolation of radioactivity concentrations (kBq/cc) measured from the arterial blood samples. Radiometabolite analysis was performed using our automated column switching radio-high performance liquid chromatography (radioHPLC) system (*23*,*24*). In short, arterial plasma was injected onto the column switching radioHPLC and initially trapped on a catch column

(Waters Oasis HLB 30 μm) using mobile phase consisting of 99:1 H_2O:MeCN at 1 mL/min (Waters 515 pump). After four minutes, the catch column was backflushed with 75/25 0.1 M ammonium formate/MeCN at 1 mL/min (second Waters 515 pump) and directed onto a Waters XBridge BEH C18 (130 Å, 3.5 μm, 4.6 mm x 100 mm) analytic column. Eluent was collected in 1 min intervals and subsequently assayed for radioactivity using a Wallac Wizard 1470 gamma counter. After background radioactivity subtraction, radioactivity eluting in the ^{18}F-T807 peak was divided by the total activity and multiplied by 100% for calculation of percent parent in plasma (%PP).

Standardized uptake value (SUV) time courses of radioactivity in whole blood were generated for intersubject comparison by correcting absolute radioactivity concentrations (C [kBq/ml]) for subject body weight (BW [kg]) and injected dose (ID [MBq]): SUV=C/(ID/BW). All subjects underwent arterial sampling for measurement of radioactivity concentration, but due to technical problems, metabolite analysis was not performed in two subjects (S7, S8). Because metabolite analysis was not performed in two subjects, %PP time course for all subjects was fit to a single exponential decay to generate a groupwise %PP(t). Arterial input functions of ^{18}F-T807 radioactivity concentration in plasma were generated by correcting plasma radioactivity concentration for ^{18}F-T807 metabolism using the groupwise %PP(t) $C_P(t) = C_P^{total}(t) \times \%PP(t)/100\%$. Finally, ^{18}F-T807 arterial SUV time courses were generated for intersubject comparisons.

Compartmental Modeling With Plasma Input Functions

Compartmental modeling was performed, using in-house developed software (MatLab), for estimation of total volume of distribution V_T and other kinetic parameters using $C_P(t)$ as the input function. Analyses were implemented on a regional basis using the conventional one- and two-tissue compartment models with a fixed vascular fraction ($f_V = 0.07$) (1T, 2T) or a variable f_V (1Tv, 2Tv) considered an additional parameter (*25*). For completeness, two-tissue compartment models with irreversible binding (2T-irrev, 2Tv-irrev) – i.e., with the binding dissociation rate constant k_4 set to zero – were also examined.

For models with reversible binding, the outcome of primary interest was the macroparameter V_T, the total volume of distribution, reflecting the equilibrium ratio of radiotracer concentration in the tissue vs. plasma (*25*). For one-tissue models, the total volume of distribution is expressed in terms of estimated kinetic parameters by $V_T=K_1/k_2$; for two-tissue models, the relationship is given by $V_T =(K_1/k_2)(1+k_3/k_4)$.

Graphical Analysis With Plasma Input Functions

Graphical methods with plasma input functions are alternative techniques for estimation of V_T in which linear regression is applied to an integral transformation of the measured dynamic data. We investigated Logan graphical method (*26*) and multilinear analysis 1 (MA1) (*27*) in this work. The optimal choice for the cutoff time *t** was assessed empirically by repeating analyses for a range of *t** values (20 to 110 minutes in 5 minute increments) and then assessing the time stability of V_T estimates as well as visually examining the quality of the resulting line fits to determine the earliest cutoff time that was applicable for all subjects and regions measured.

Reference Region Based Analyses

Reference region based analyses of ^{18}F-T807 uptake were performed using the cerebellum (excluding the vermis) as a reference tissue. Distribution volume ratio (DVR) (equivalent to V_T/V_{ND}, assuming a valid reference tissue) was estimated using the Logan graphical method with reference region input function (*28*). The optimal *t** was determined as for the plasma Logan method by systematically varying the cutoff time and assessing linearity of the transformed data and stability of resulting DVR estimates.

The most simplified analysis method surveyed in this work was the SUVR of radioactivity concentration in a tissue region divided by the radioactivity concentration in the reference tissue. The cerebellum was again used as the reference tissue and SUVR was calculated from PET data acquired 80-100 minutes post-injection ($SUVR_{80\text{-}100}$).

Estimates of Logan DVR and SUVR were compared to equivalents of DVR from compartmental modeling with arterial inputs, namely V_T^{tissue}/V_T^{ref}.

Parametric Mapping

Dynamic PET images were smoothed by application of a 3 mm (FWHM) Gaussian filter. Logan analysis with plasma input were then applied in a voxel-by-voxel fashion to produce parametric maps of V_T^{tissue}/V_T^{ref} to allow a comparison with voxelwise parametric images generated using the Logan method with reference tissue input and static $SUVR_{80\text{-}100}$.

Statistical Analysis

The goodness of fit for alternative compartmental models was compared within each data set using the Akaike information criterion $AIC = n\ln(RSS/n) + 2k$, where n is the number of time frames, RSS is the residual sum of squares and k is the number of model parameters (*29*). We utilized AIC weights to assign to each evaluated model the probability that that particular model gave the highest quality fit to the data. Weights were calculated as $AIC_{weight,i} = e^{-\frac{1}{2}\Delta_i} / \sum_k e^{-\frac{1}{2}\Delta_k}$, where i indexes the individual models and k indicates the total number of models considered (six, in our case) and $\Delta_i = AIC_i - AIC_{min}$ with AIC_{min} defined as the minimum AIC value for the time activity curve being evaluated (*30*). To enable group comparison of model preference, median AIC weights are reported in this paper.. Statistical processing was performed using GraphPad Prism software. Quantification methods of ^{18}F-T807 were compared using the coefficient of determination and t distribution of the Fisher transformation to generate p values for linear regressions. All data are reported as mean +/- s.d. unless otherwise noted.

RESULTS

Imaging Procedures

PET and MR imaging procedures were performed in nine subjects from three status groups. Subject information is shown in Table 1. The mean and standard deviation of the administered mass of ^{18}F-T807 was 1.0 ± 0.5 μg (range, 0.4–2.0). The mean administered activity was 176 ± 23 MBq (range, 121–196 MBq).

Radioactivity In Arterial Blood

WB to plasma radioactivity concentration rapidly reached equilibrium averaging 0.98 ± 0.04 by 1 minute post injection as shown in Figure 1.A. WB radioactivity time course showed consistency across subjects as shown in Figure 1.B. A slight increase in WB SUV was observed after about 30 minutes post injection.

An example radioHPLC fraction chromatogram for the 15-minute sample from a representative subject (S6) is shown in Figure 1.C. As confirmed by direct injection of an aliquot of the radiotracer onto the system, ^{18}F-T807 began eluting from the column switching radioHPLC at 12 minutes. Figure 1.D. shows concentration over time of the three radioactivity fractions. %PP of ^{18}F-T807 over time was well described by a single exponential fit with a half-life of 17.0±4.2 minutes. Mean and standard deviation of %PP time course is shown in Figure 1.E.

^{18}F-T807 radioactivity concentration time course in plasma is shown in Figure 1.F. After five minutes post injection, the average metabolite-corrected plasma data were described well by a biexponential function ($T_{1/2}$s = 2.4±0.5 and 18.1±5.8 minutes). After 10 minutes, the coefficient of variation (CV) in ^{18}F-T807 SUV in plasma across subjects was 17±3.5%. No differences in metabolite corrected plasma SUV were discernible between control subjects, subjects with a history of TBI, and MCI subjects.

--Insert Figure 1 here--

Region Of Interest Analysis

Peak SUV in gray matter averaged 2.4 ± 0.27 and was greater than 2 for all subjects. In white matter, peak SUV averaged 1.92 ± 0.17 for all subjects. Shown in Figure 2 are regional TACs from different brain regions for a representative control and two subjects demonstrating tau pathology. For the control subject, TACs had relatively homogeneous kinetics and converged to similar values by about 40 minutes. For the two subjects demonstrating tau pathology, TACs showed regionally enhanced uptake and greater inter-region heterogeneity in kinetics.

--Insert Figure 2 here--

Figure 2D shows cerebellar TACs for all subjects. The CB exhibited fast wash-in of radioactivity with high initial peak SUV (≥2) and rapid clearance (SUV <1 by 60 minutes). SUV values reached reasonable convergence by about 60 minutes. As observed in Figure 2D, subjects with a history of TBI exhibited somewhat reduced peak SUV compared to the control and MCI subjects.

Fits to regional TACs for the 2Tv models are shown in Figure 2A-C (fits for 1Tv models are shown in Supplemental Figure 2). In MCI subjects, high preference for the 2Tv reversible model was observed ($AIC_{weight,median}$ =1). In control subjects, preference for the 2Tv reversible model was maintained with $AIC_{weight,median}$ =0.73. Interestingly, for the TBI subjects, model preference seemed to shift towards the 2Tv irreversible model, with $AIC_{weight,median}$ =0.05 for the reversible and $AIC_{weight,median}$ =0.48 for the irreversible model. The 2Tv reversible model was selected as the compartmental method of choice because it provided good fits in all data sets (notably including those showing high uptake), was statistically preferred in a majority of data sets, and provides an outcome consistent with our understanding of the tracer's binding properties. Compartmental results reported throughout the remainder of this paper are from this model unless otherwise noted. Omission of the vascular contribution (f_V) as a parameter greatly

reduced AIC weights ($AIC_{weight,median}$=0). Regional V_T estimates from the 2Tv model are shown in Figure 3.A. and in Supplemental Table 2 Cerebellum showed lowest variability in V_T (4.1±0.5; CV=11.8%) despite larger variation in SUV (see Figure 2D and text earlier in this section). No significant differences in cerebellar V_T, K_1, or k_2 were found between the subject groups. Cerebellar K_1 was stable at 0.26 ± 0.06 ml·min^{-1}·cm^{-3}) with higher variability found in k_2 (0.17 ± 0.13 min^{-1}).

--Insert Figure 3 here--

Logan (*26*) and MA1 (*27*) graphical methods resulted in estimates of V_T highly correlated with those from 2Tv. The Logan plot for one subject with a range of uptake is shown in Figure 3B demonstrating a reasonable level of linearization by t^* of 30 minutes. As shown in Figure 3C-D, high correlation was found between both graphical methods and the estimates of V_T from compartmental analysis (Logan: R^2=0.97, p<0.0001; MA1: R^2=0.97, p<0.0001). Additionally, as shown in Supplemental Figure 3, estimates of Logan V_T correlated well with MA1 V_T (Logan: R^2=0.99, p<0.0001)

Reference region based analysis was performed using the CB due to the high consistency observed in V_T across the subjects. Logan analyses performed with t^* systematically varied between 20 and 110 minutes demonstrated stabilization in DVR over all regions by approximately 55 minutes. A representative Logan plot is shown in Figure 4A demonstrating linearization is reached by the 55 min cutoff time (indicated by the large circles) even in the higher binding regions. A comparison of 2Tv V_T/V_T^{ref} and Logan DVR is shown in Figure 4B indicates high correlation (R^2=0.96, p<0.0001) though with some negative bias at high values. A comparison of 2Tv V_T/V_T^{ref} and $SUVR_{80\text{-}100}$ shows similarly high correlation (R^2=0.96, p<0.0001; Figure 4C) however no bias is evident across the range of observed values. In white matter, $SUVR_{80\text{-}100}$ averaged 1.15 ± 0.1 over all control subjects.

Figure 5 shows SUVR time courses along with Logan DVR and 2Tv V_T/V_T^{ref} estimates for 3 regions in one control subject and one MCI subject. The control subject reaches a plateau in all regions within about 20 minutes. In the higher uptake regions of the MCI subject, a plateau begins by approximately 80-90 minutes.

--Insert Figure 4 here--

--Insert Figure 5 here--

^{18}F-T807 Parametric Images

^{18}F-T807 Logan V_T^{tissue}/V_T^{ref}, Logan DVR, and $SUVR_{80\text{-}100}$ maps generated using the CB as a reference region are shown in Figure 6 for a control subject, one subject who had been in a car accident approximately 10 years prior to imaging with ^{18}F-T807, and two MCI subjects. Also displayed is the subjects MPRAGE image in standardized space of the same slice for localization. Overall features are comparable for the alternative PET analysis methods, however some discrepancies can be observed. For instance, $SUVR_{80\text{-}100}$ has a generally noisier appearance and exhibits relatively higher signal in white matter than either of the kinetic analysis methods, a phenomenon most prominent in the control and TBI subjects. Conversely, signal in the basal ganglia is reduced in the $SUVR_{80\text{-}100}$ images as compared to maps obtained by Logan regression methods; similar patterns are present elsewhere, notably in occipital lobe of one MCI subject (S8) and in the frontal cortex of the other (S9).

--Insert Figure 6 here--

DISCUSSION

There has been a great effort toward the development of PET imaging agents for tau pathology due to the implication of tau in neurodegenerative diseases such as AD and TBI. ^{18}F-T807 was developed for PET imaging of tau pathology and has been widely used in research studies and is currently undergoing clinical trials as a diagnostic PET radiotracer. Despite its expanding use, a full characterization of ^{18}F-T807's pharmacokinetics has yet to be investigated. The goal of this work was to provide an initial in vivo pharmacokinetic evaluation of the tau radiotracer ^{18}F-T807 using metabolite corrected arterial input functions and dynamic PET imaging data. Herein, we evaluate subjects who present a range of ^{18}F-T807 uptake in order to properly assess different methods for quantification and to provide a preliminary analysis of simplified reference region based methods.

^{18}F-T807 In Blood

Radioactivity concentration in whole blood demonstrated rapid clearance with approximately 4% of the initial peak radioactivity present at 20 minutes post injection. Nonpolar radioactive metabolites detected using radio-HPLC were minimal. Furthermore, high intersubject consistency was found in ^{18}F-T807 metabolism and ^{18}F-T807 breakdown resulted in primarily polar metabolites. For this analysis, we found a group %PP function to be adequate

due to the high similarity in ^{18}F-T807 metabolism between subjects as the group %PP vs subject specific %PP correction resulted in highly concordant estimates of V_T as shown in Supplemental Figure 4 ($R^2 = 0.99, y = 1.02x - 0.09, p < 0.0001$).

CB As A Reference Region

For simplified quantification methods beyond SUV, a reference region void of radiotracer target is necessary to provide a surrogate for the arterial input function. Of the regions examined in this work, the CB showed the lowest variability in V_T and the lowest overall V_T. Additionally, the CB showed fast wash-in and fast clearance resulting in low overall specific binding of ^{18}F-T807. In the control and TBI subjects, some regions exhibited DVR values < 1, however, regional DVR in MCI subjects were ≥ 1. Other potential reference regions examined in this work included parts of the brainstem comprising of the pons and medulla, however, high variability in total volume of distribution was found in these areas. This preliminary analysis supports the use of the cerebellum as the most appropriate reference region. Due to the particular staging of tau in Alzheimer's disease, we do not anticipate the cerebellum will comprise of significant tau deposition (*17*,*31*,*32*) . Subjects with TBI on the other hand could potentially present with tau in a less predictable manner. Ultimately, a larger study set will be required to fully validate the cerebellum as a reference region in AD subjects and subjects with TBI.

Simplified Approaches For Quantification Of ^{18}F-T807 Uptake

We examined simplified approaches for quantification of ^{18}F-T807 uptake including the Logan method for estimation of DVR and SUVR. High correlation was observed between compartmental modeling based estimates of V_T/V_T^{ref} using the CB as a reference and estimates of Logan DVR and SUVR indicating reference region based estimates of ^{18}F-T807 uptake will be adequate in place of full arterial sampling and compartmental modeling. Examination of truncated imaging times on Logan DVR estimation showed 90 minutes of data were comparable to those from 120 minutes, whereas 60 minutes of data yielded biases of >10%. SUVR overestimated V_T/V_T^{ref} when compared to the Logan DVR method; however, reasons for this overestimation have been discussed in the literature (*33*,*34*). Plots of SUVR time course suggested at least 80-100 minutes of time would be required for high ^{18}F-T807 binding regions to reach pseudoequilibrium with the reference region which is similar to previously suggested SUVR imaging times (*12*). Comparison of SUVR maps using 40-60 minutes, 80-100 minutes, and 100-120 minutes

are shown in Supplemental Figure 5. As demonstrated, SUVR from 80-100 minutes, 100-120 minutes are comparable, but SUVR from 40-60 haven't reached peak values. In the lower binding subjects and regions, however, about 30 minutes are necessary for SUVR to become stable. These results provide compelling evidence that late static imaging may serve in place of full dynamic imaging with arterial blood sampling.

^{18}F-T807 Uptake And Distribution

^{18}F-T807 demonstrated high brain penetration with peak SUV immediately after injection of greater than two in grey matter. Additionally, K_1 averaged 0.25 across subjects and regions indicating moderate high brain extraction. Previous work has shown THK5105 to have high nonspecific white matter binding (*11*). This nonspecific uptake is attributed to β-sheet structures in myelin and could be problematic for quantification of tau. Peak SUV of ^{18}F-T807 in white matter averaged 1.92 and $SUVR_{80\text{-}120}$ minutes in white matter was 1.15 ± 0.1 indicating mild nonspecific white matter binding. In contrast to ^{18}F-T808, uptake in the skull was minimal for ^{18}F-T807 (Supplemental Figure 6) indicating low defluorination.

As the parametric images in Figure 6 indicate, ^{18}F-T807 uptake can be quantified reliably using graphical methods or SUVR. Images of SUVR were the lowest quality with apparent uptake in white matter that was not observed in the V_T or DVR maps, however, SUVR seemed to be adequate for delineation and estimation of relative uptake of ^{18}F-T807.

Overall, distribution of ^{18}F-T807 in the control subject was generally uniform with no cortical areas expressing high distribution. Although not explicitly examined in this work, intersubject heterogeneity in uptake was observed in subcortical areas, e.g., the thalamus and putamen. Similar off target binding results have been observed (*35*). In addition, our previous autoradiography work demonstrated off target binding to neuromelanin and melanin containing cells as well as hemorrhagic lesions (*17*). Further examination of this off-target subcortical binding is warranted. The subject with a severe TBI due to an automobile accident expressed one region of very high uptake protruding from the posterior regions of the corpus callosum into the posterior cingulate gyrus possibly as a result of brain injury. Finally, the two MCI subjects demonstrated different distributions in uptake. S8 had highest uptake in the occipital regions. Subject S9 on the other hand demonstrated high ^{18}F-T807 uptake in areas associated with staging of tau in Alzheimer's disease (*31*) including temporal, parietal, posterior cingulate, and precuneus regions.

Study Limitations

This work included some limitations including no test-retest data. However, we observed low variability in blood data and cerebellar V_T across subjects indicating test-retest would also be low. Use of a groupwise ^{18}F-T807 metabolism correction is a limitation and a full examination of intersubject variability in ^{18}F-T807 metabolism would be helpful to determine if there are differences between groups (MCI, TBI, and controls). Additionally, we only examined tauopathies related to MCI subjects and subjects with history of brain injury. A thorough investigation of ^{18}F-T807 kinetics in subjects with related tauopathies (e.g., frontotemporal dementia) will be necessary to determine the ^{18}F-T807 kinetic properties found in this work translate to other tau-related diseases. Even though for most subjects a two-tissue reversible model was preferred based on AIC, we found preference for the irreversible model in our TBI subjects. A full examination of ^{18}F-T807 kinetics in TBI subjects with a range of binding is needed to investigate this apparent discrepancy. Finally, our overall subject number was low, however, the subjects examined in this work had a wide range of dynamic ^{18}F-T807 uptake allowing evaluation of ^{18}F-T807's kinetics in subjects with the highest binding expected as indicated by Johnson and colleagues who found highest ^{18}F-T807 posterior cingulate SUVRs between 2 to 2.5 (*18*).

CONCLUSION

^{18}F-T807 showed low intersubject variability in metabolism rate and overall rapid clearance in plasma. Two-tissue reversible compartmental modeling using ^{18}F-T807 arterial input function resulted in close agreement with linearized methods of V_T estimation using both Logan (*26*) and MA1 (*27*). The cerebellum exhibited properties required for use as a reference region in place of arterial sampling. These initial results show promise for a simplified reference region based protocol negating arterial sampling and using late static imaging with the goal of shorter scan times. Reference region based methods of quantification including Logan DVR with a t*=55 minutes and SUVR from 80-100 minutes tracked closely with compartmental modeling based outcome measures using arterial plasma input functions. Lastly, these results demonstrate ^{18}F-T807 possesses the properties necessary for quantification of tau using PET imaging. Further studies will be needed to fully characterize the use of the cerebellum as a valid reference region in a heterogenous population.

REFERENCES

1. Iqbal K, Liu F, Gong CX, Grundke-Iqbal I. Tau in Alzheimer disease and related tauopathies. *Curr Alzheimer Res.* 2010;7:656-664.

2. James OG, Doraiswamy PM, Borges-Neto S. PET Imaging of Tau Pathology in Alzheimer's Disease and Tauopathies. *Front Neurol.* 2015;6:38.

3. Hyman BT, Phelps CH, Beach TG, et al. National Institute on Aging-Alzheimer's Association guidelines for the neuropathologic assessment of Alzheimer's disease. *Alzheimers Dement.* 2012;8:1-13.

4. Goldstein LE, Fisher AM, Tagge CA, et al. Chronic traumatic encephalopathy in blast-exposed military veterans and a blast neurotrauma mouse model. *Science translational medicine.* 2012;4:134ra160.

5. McKee AC, Cantu RC, Nowinski CJ, et al. Chronic traumatic encephalopathy in athletes: progressive tauopathy after repetitive head injury. *J Neuropathol Exp Neurol.* 2009;68:709-735.

6. Ariza M, Kolb HC, Moechars D, Rombouts F, Andres JI. Tau Positron Emission Tomography (PET) Imaging: Past, Present, and Future. *J Med Chem.* 2015;58:4365-4382.

7. Agdeppa ED, Kepe V, Liu J, et al. Binding characteristics of radiofluorinated 6-dialkylamino-2-naphthylethylidene derivatives as positron emission tomography imaging probes for beta-amyloid plaques in Alzheimer's disease. *The Journal of neuroscience : the official journal of the Society for Neuroscience.* 2001;21:RC189.

8. Hashimoto H, Kawamura K, Igarashi N, et al. Radiosynthesis, photoisomerization, biodistribution, and metabolite analysis of 11C-PBB3 as a clinically useful PET probe for imaging of tau pathology. *J Nucl Med.* 2014;55:1532-1538.

9. Kimura Y, Ichise M, Ito H, et al. PET Quantification of Tau Pathology in Human Brain with 11C-PBB3. *J Nucl Med.* 2015;56:1359-1365.

10. Harada R, Okamura N, Furumoto S, et al. 18F-THK5351: A Novel PET Radiotracer for Imaging Neurofibrillary Pathology in Alzheimer's Disease. *J Nucl Med.* 2015.

11. Okamura N, Furumoto S, Fodero-Tavoletti MT, et al. Non-invasive assessment of Alzheimer's disease neurofibrillary pathology using 18F-THK5105 PET. *Brain.* 2014;137:1762-1771.

12. Chien DT, Bahri S, Szardenings AK, et al. Early clinical PET imaging results with the novel PHF-tau radioligand [F-18]-T807. *Journal of Alzheimer's disease : JAD.* 2013;34:457-468.

13. Xia C-F, Arteaga J, Chen G, et al. [(18)F]T807, a novel tau positron emission tomography imaging agent for Alzheimer's disease. *Alzheimer's & dementia : the journal of the Alzheimer's Association.* 2013;9:666-676.

14. Zhang W, Arteaga J, Cashion DK, et al. A highly selective and specific PET tracer for imaging of tau pathologies. *Journal of Alzheimer's disease : JAD.* 2012;31:601-612.

15. Chien DT, Szardenings AK, Bahri S, et al. Early clinical PET imaging results with the novel PHF-tau radioligand [F18]-T808. *J Alzheimers Dis.* 2014;38:171-184.

16. Shoup TM, Yokell DL, Rice PA, et al. A concise radiosynthesis of the tau radiopharmaceutical, [(18) F]T807. *Journal of labelled compounds & radiopharmaceuticals.* 2013;56:736-740.

17. Marquie M, Normandin MD, Vanderburg CR, et al. Validating novel tau positron emission tomography tracer [F-18]-AV-1451 (T807) on postmortem brain tissue. *Ann Neurol.* 2015;78:787-800.

18. Johnson KA, Schultz A, Betensky RA, et al. Tau PET imaging in aging and early Alzheimer's disease. *Ann Neurol.* 2015.

19. Brant-Zawadzki M, Gillan GD, Nitz WR. MP RAGE: a three-dimensional, T1-weighted, gradient-echo sequence--initial experience in the brain. *Radiology.* 1992;182:769-775.

20. Alpert NM, Berdichevsky D, Levin Z, Morris ED, Fischman AJ. Improved methods for image registration. *Neuroimage.* 1996;3:10-18.

21. Grabner G, Janke AL, Budge MM, Smith D, Pruessner J, Collins DL. Symmetric atlasing and model based segmentation: an application to the hippocampus in older adults. *Medical image computing and computer-assisted intervention : MICCAI International Conference on Medical Image Computing and Computer-Assisted Intervention.* 2006;9:58-66.

22. Jenkinson M, Beckmann CF, Behrens TEJ, Woolrich MW, Smith SM. FSL. *NeuroImage.* 2012;62:782-790.

23. Collier T, Normandin M, El Fakhri G, Vasdev N. Automation of column-switching HPLC for analysis of radiopharmaceuticals and their metabolites in plasma. *Society of Nuclear Medicine Annual Meeting Abstracts.* 2013;54:1133.

24. Hilton J, Yokoi F, Dannals RF, Ravert HT, Szabo Z, Wong DF. Column-switching HPLC for the analysis of plasma in PET imaging studies. *Nucl Med Biol.* 2000;27:627-630.

25. Innis RB, Cunningham VJ, Delforge J, Fujita M, Gjedde A, Gunn RN. Consensus nomenclature for in vivo imaging of reversibly binding radioligands. *J Cereb Blood Flow Metab.* 2007;27:1533-1539.

26. Logan J, Fowler JS, Volkow ND, et al. Graphical analysis of reversible radioligand binding from time-activity measurements applied to [N-11C-methyl]-(-)-cocaine PET studies in human subjects. *J Cereb Blood Flow Metab.* 1990;10:740-747.

27. Ichise M, Toyama H, Innis RB, Carson RE. Strategies to improve neuroreceptor parameter estimation by linear regression analysis. *J Cereb Blood Flow Metab.* 2002;22:1271-1281.

28. Logan J, Fowler JS, Volkow ND, Wang GJ, Ding YS, Alexoff DL. Distribution volume ratios without blood sampling from graphical analysis of PET data. *J Cereb Blood Flow Metab.* 1996;16:834-840.

29. Akaike H. A new look at the statistical model identification. *IEEE Transactions on Automatic Control.* 1974;19:716-723.

30. Burnham KP, Anderson DR, Burnham KP. *Model selection and multimodel inference : a practical information-theoretic approach*. 2nd ed. New York: Springer; 2002.

31. Braak H, Braak E. Neuropathological stageing of Alzheimer-related changes. *Acta neuropathologica.* 1991;82:239-259.

32. McKee AC, Stern RA, Nowinski CJ, et al. The spectrum of disease in chronic traumatic encephalopathy. *Brain.* 2013;136:43-64.

33. Slifstein M. Revisiting an old issue: the discrepancy between tissue ratio-derived binding parameters and kinetic modeling-derived parameters after a bolus of the serotonin transporter radioligand 123I-ADAM. *J Nucl Med.* 2008;49:176-178.

34. Carson RE, Channing MA, Blasberg RG, et al. Comparison of Bolus and Infusion Methods for Receptor Quantitation: Application to 18F-Cyclofoxy and Positron Emission Tomography. *J Cereb Blood Flow Metab.* 1993;13:24-42.

35. Shcherbinin S, Schwarz AJ, Joshi AD, et al. Kinetics of the tau PET tracer 18F-AV-1451 (T807) in subjects with normal cognitive function, mild cognitive impairment and Alzheimer's disease. *J Nucl Med.* 2016.

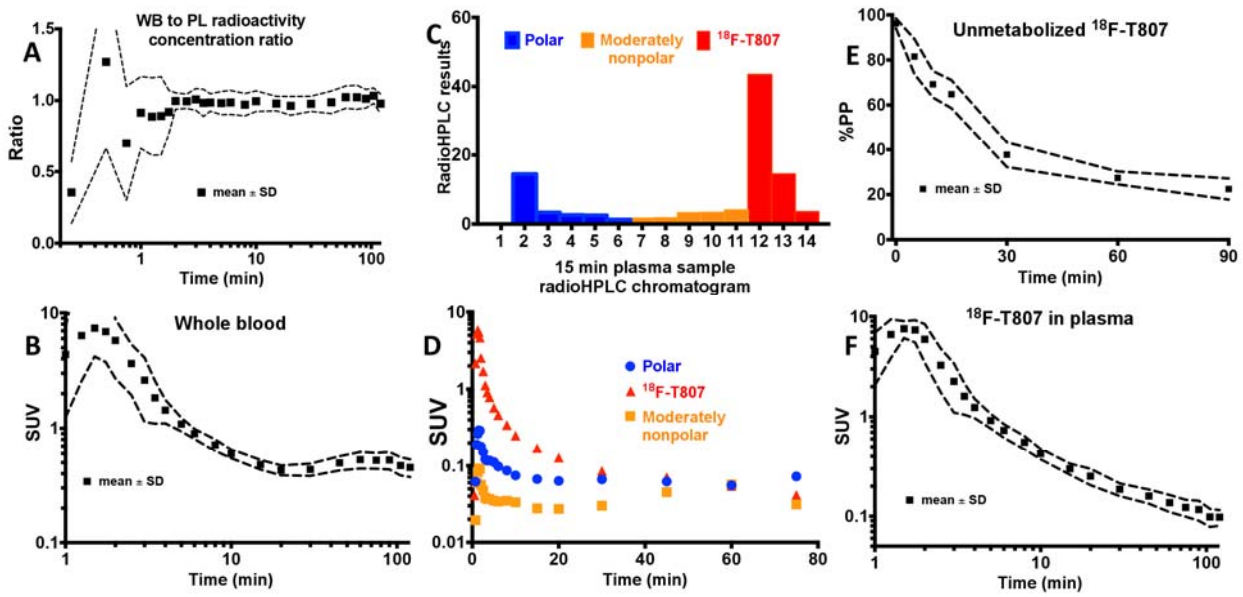

Figure 1: Arterial blood measurements. (A) Plot of whole blood to plasma radioactivity concentration ratio. (B) Whole blood SUV time course. (C) Reverse phase radioHPLC chromatogram from the 15-minute plasma sample in subject S6 with polar, moderately nonpolar, and ^{18}F-T807 delineated. (D) Time course of polar, slightly nonpolar, and ^{18}F-T807 components as depicted in (C). (E) Percent parent plasma (%PP) of ^{18}F-T807. (F) ^{18}F-T807 SUV time course in plasma. A,B,E, and F show mean and standard deviation across all subjects, whereas C and D show data from a representative subject.

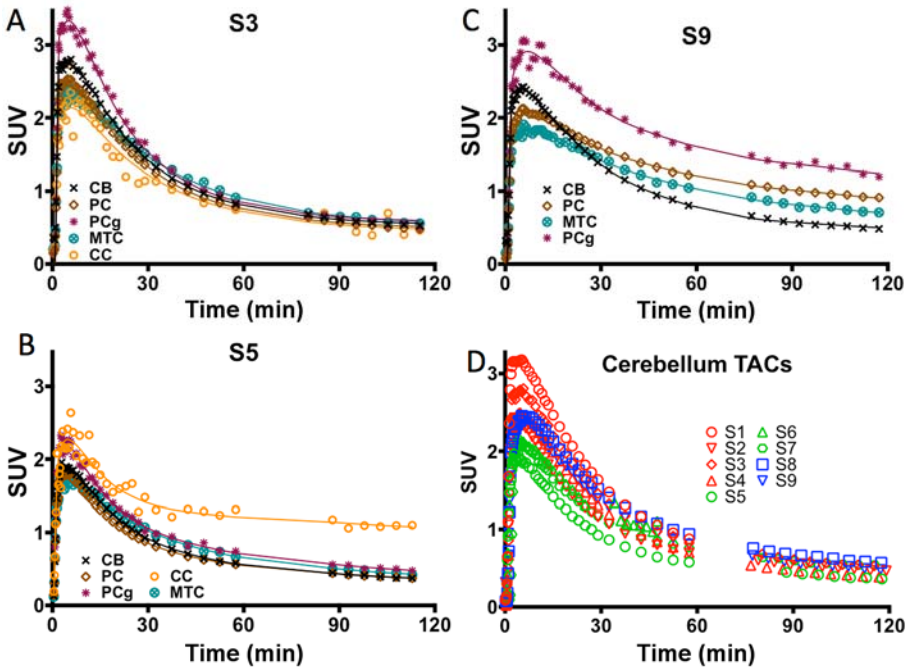

Figure 2: (A-C) Time activity curves and 2Tv (solid lines) fits for a control subject S3, a subject with history of traumatic brain injury S5, and a MCI subject S9. (D) SUV PET measured time course in the CB for all subjects.

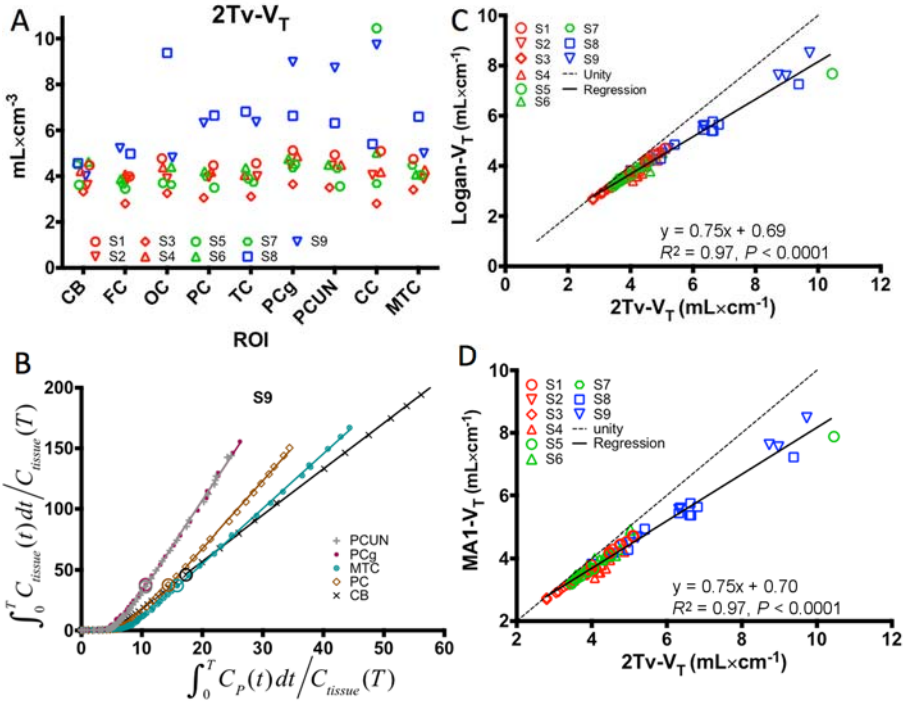

Figure 3: Results from arterial input function based analyses. (A) Regional V_T estimates from the 2Tv compartmental model in the cerebellum (CB), frontal cortex (FC), occipital cortex (OC), parietal cortex (PC), temporal cortex (TC), posterior cingulate gyrus (PCg), precuneus (PCUN), subject specific ROI in the corpus callosum (CC), and the mesial temporal cortex (MTC). (B) Demonstration of Logan plot linearization in MCI subject S9 for estimation of V_T. Large circles depict the 30 minute t^* point. Note that the axes were truncated to enhance visualization of the higher binding regions. (C-D) Comparison of 2Tv and graphical estimates of V_T using either Logan analysis (C) or MA1 (D). In A,C, and D, red markers designate control subjects, green markers correspond to TBI subjects, and blue markers indicate MCI subjects.

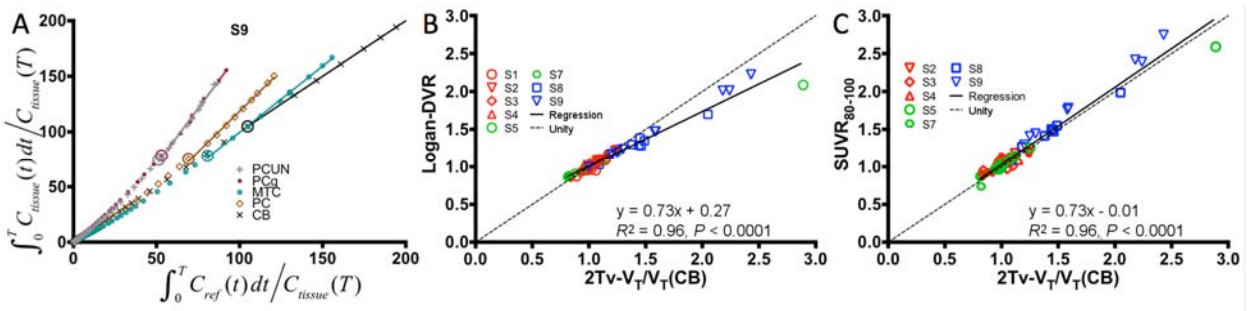

Figure 4: Results from reference region based analyses with cerebellar input functions. (A) Demonstration of Logan plot linearization in MCI subject S9 for estimation of distribution volume ratio (DVR). Large circles depict the 55 minute *t** point. Note that the axes were scaled down to enhance the visualization of the higher uptake regions. Comparison of Logan DVR (B) and $SUVR_{80\text{-}100}$ (C) against indirect calculations of DVR given V_T/V_T^{REF} with distribution volumes estimated by compartmental modeling with arterial input functions and V_T^{REF} corresponding to the cerebellum.

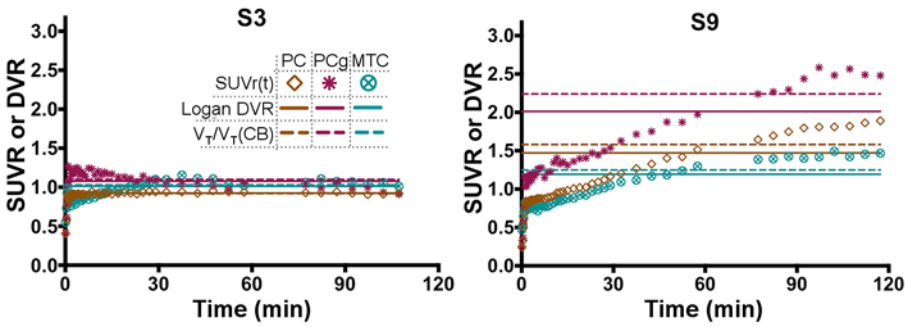

Figure 5: SUVR time courses (symbols), DVR estimated directly by Logan regression with reference region inputs (horizontal solid lines), and indirect estimates of DVR given by V_T/V_T^{REF} from compartmental modeling with arterial inputs (horizontal dashed lines) for a control subject (S3) and an MCI subject (S9).

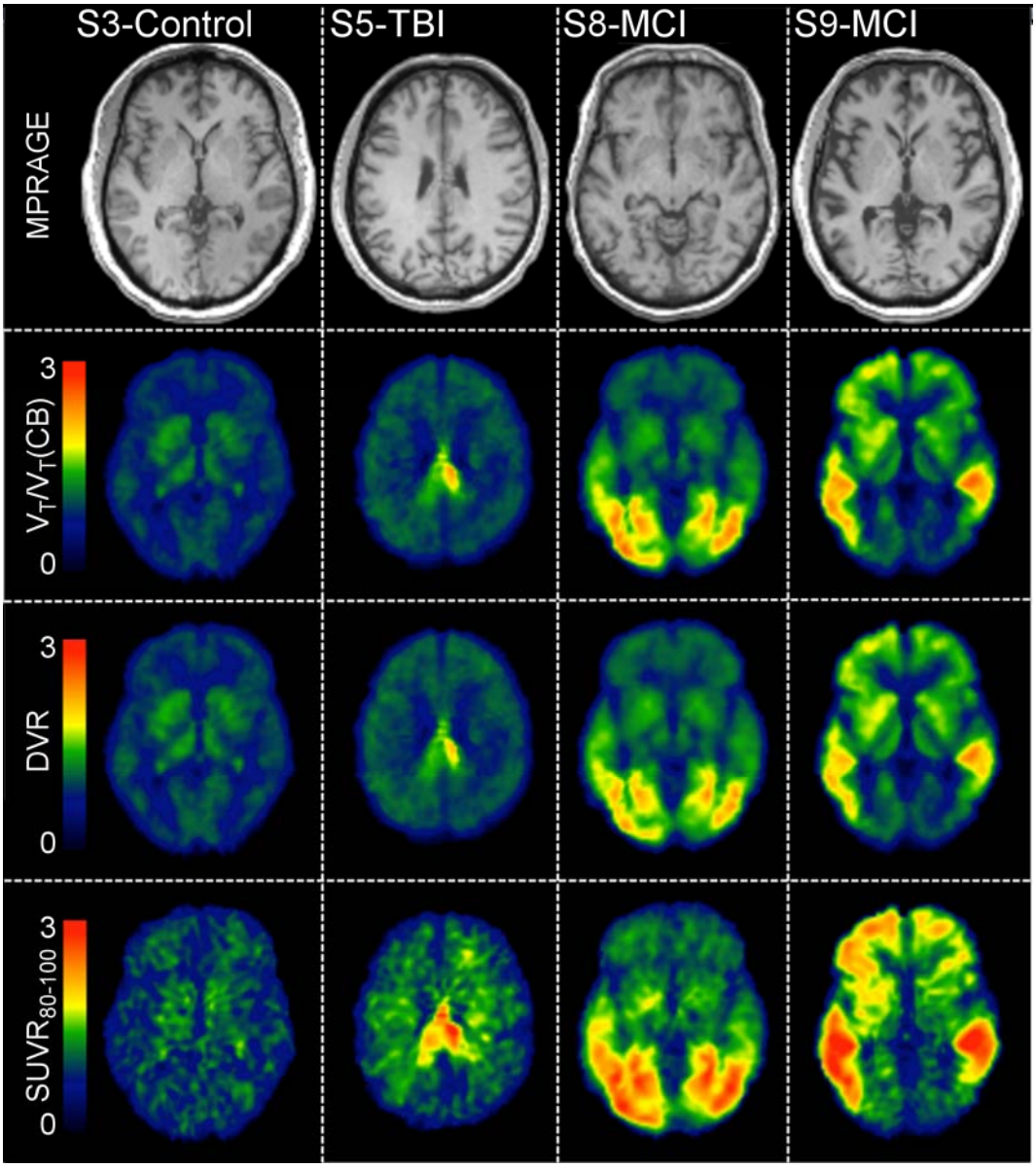

Figure 6: MPRAGE in template space and parametric images of indirect calculation of DVR using Logan ($V_T/V_T(CB)$), Logan DVR, and SUVR in a control subject (S3), a subject with history of traumatic brain injury (S5), and two subjects with MCI (S8 and S9).

Subject	Status	Age(y)	Sex	mass (kg)	BMI(kg/m^2)	Years since TBI exposure
S1	CNTL	60	M	93	28.5	N.A.
S2	CNTL	29	M	74	22.2	N.A.
S3	CNTL	47	M	136	38.5	N.A.
S4	CNTL	53	M	70	22	N.A.
S5	TBI[A]	34	M	68	24.9	10
S6	TBI[A]	31	M	100	26.7	10
S7*	TBI[B]	55	M	105	28.2	20
S8*	MCI[C]	71	F	54	23.4	N.A.
S9	MCI[D]	72	M	83	29.3	N.A.
*radiometabolite measurements not performed, [A]car accident, [B]NFL multiple concussions, [C]MMSE=27, [D]MMSE=14						

Table 1: Subject information.